ISSN 0016-7029, Geochemistry International, 2009, Vol. 47, No. 3, pp. 231–243. © Pleiades Publishing, Ltd., 2009.
Original Russian Text © V.L. Tauson, R.G. Kravtsova, V.I. Grebenshchikova, E.E. Lustenberg, S.V. Lipko, 2009, published in Geokhimiya, 2009, No. 3, pp. 245–258.

Surface Typochemistry of Hydrothermal Pyrite: Electron Spectroscopic and Scanning Probe Microscopic Data. II. Natural Pyrite

V. L. Tauson, R. G. Kravtsova, V. I. Grebenshchikova, E. E. Lustenberg, and S. V. Lipko

Vinogradov Institute of Geochemistry, Siberian Branch, Russian Academy of Sciences, ul. Favorskogo 1a, Irkutsk, 664033 Russia

e-mail: vltauson@igc.irk.ru

Received March 3, 2008

Abstract—Pyrite crystals from gold deposits of various genetic types (mesothermal and epithermal) were examined by techniques of x-ray photoelectron and Auger electron microscopy and by scanning probe microscopy. The results confirm a conclusion made in earlier hydrothermal experiments that nonautonomous phases (NP) of variable composition occur on the surface of pyrite crystals. These phases are localized within a layer of submicrometer (nanometer) thickness (up to ~0.5 μm) within which the typochemistry of pyrite surface is pronounced. The development of sulfate on the surface of pyrite crystals from epithermal Au–Ag deposits is a typochemical feature of the origin of their ore mineralization at low temperatures and shallow depths. Supergene conditions are characterized by the presence of an oxi-hydroxide or oxide film of FeIII, which morphologically differs from the layer of a pyrite-like NP. The composition and properties of the NPs are different for pyrite from mesothermal and epithermal deposits: they are close to those of a pyrrhotite-like NP discovered on synthetic hydrothermal pyrite and contain an additional sulfite anion for pyrite from the former type of deposits and are close to sulfide–disulfide ensembles with trivalent Fe for pyrite from the latter type of deposits. Trace elements, including precious metals, can be accommodated in such a phase via the stabilization of clusters with Fe^{3+} and SO_4^{2-} in its structure. The instability of the crystallization process in epithermal environments may bring about the development of double-level nanostructure because of the structural transformation of vicinal surfaces into a set of ordered domains and the synthesis of nonautonomous "precursor" phases. Such systems can be stabilized via the excess dissolution of admixtures or the transition of the surface layer into another phase state.

DOI: 10.1134/S0016702909030021

INTRODUCTION

In our earlier publications [1, 2], we attempted to prove that the composition of the surface of mineral crystals provides a record of events in their geochemical history and characteristics of the medium from which these crystals were formed. The development of this approach seems to be fruitful for geochemistry and mineralogy, because the physicochemical analysis traditionally applied in these fields as a complex of techniques for studying physical systems is characterized by the "complete lack of a historical approach" [3], and this approach cannot be borrowed from anywhere else than the geological reality, an element of which is the surface of an individual mineral.. These surfaces can accumulate components that are absent from the crystal volume, because the composition, structure, and even the state of chemical bonds in surface layers notably differ from those in the crystal volume. The first paper of this series [4] presented data on the discovery of a nonautonomous phase (NP) in a ~300-nm-thick layer on the natural surface of hydrothermally synthesized pyrite crystals. The natural surface of hydrothermal pyrite is chemically modified (as compared to the crystal volume) into a phase of variable composition that resembles pyrrhotite but is characterized by broader compositional variations toward FeS_2. The "basic" structure of the NP is a layer of variable composition $Fe^{2+}[S, S_2, S_n]^{2-}$ in which the S/S_2 ratio varies within a fairly broad range. The typomorphism of the pyrite surface is based on the ability of this phase to provide a record of the conditions under which the crystal grew with respect to two major factors: the purity of the system (the occurrence of additional phases, including virtual ones, i.e., potentially possible phases of minor elements) and sulfur fugacity. The most typical spectroscopic feature of the NP on pyrite is the XPS peak FeII $2p_{3/2}$ at ~710 eV, whose intensity is sometimes greater than that of the head peak of low-spin FeII in the pyrite structure (~707 eV). The spectrum of Fe $2p_{2/3}$ of the pyrrhotite-like NP (PoNP) resembles the analogous spectrum of crystals of nonstoichiometric pyrrhotite that were hydrothermally synthesized close to the pyrite stability field [5], except that the peak of the NP is shifted toward a lower energy value. Our earlier data

[4] indicate that the position of this peak, which was ascribed to FeII–S (PoNP), varies from ~709 to ~711 eV, which is likely controlled by the stoichiometry of the surface layer and its qualitative composition and can also depend on its structure. It should be mentioned that the surface of pyrrhotite was also found to contain an NP [5] that may include elements of the pyrite structure. This is validated by the fact that the XPS spectrum of Fe 2p includes a broad peak with a maximum near 707 eV at the standard position of the FeII peak coordinated with disulfide ligands in pyrite.

The goal of our research was to study the surface of a pyrite crystal from hydrothermal gold deposits of various genesis and to compare these results with our earlier data on synthetic pyrite [4]. This enabled us to estimate the geochemical role of the surface NP and the nonstoichiometric surface layer in the accommodation of minor elements that are incompatible with the pyrite structure but can easily "adjust" themselves to the less rigid structure of the NP. Because of the diversity of S speciation (S^{2-}, S_2^{2-}, S_n^{2-}, , and sulfoxi anions) and the absence of strict constraints in terms of space and bond length (because of the variable sulfide/disulfide ratio), many of them can be accommodated in the surface layer but are incompatible with the crystalline matrix.

MATERIALS AND METHODS

Pyrite samples were collected from mineralized veins and wall-rock metasomatites at the Zun-Kholba mesothermal deposit in the Eastern Sayan Range and at the epithermal Au–Ag deposits Dal'nee and Oroch in the northern Ol'khon area and Pokrovskoe in Amur oblast [1].

The ore mineralization of the Zun-Kholba deposit in the Urik–Kitoi ore mining district belongs to the quartz–sulfide mesothermal type [6]. The deposit is spatially restricted to the boundary between the Archean Gargan block of Archean amphibolites and gneisses, its overlying Proterozoic terrigenoussedimentary cover, a Late Riphean ophiolite allochthon, and the Late Riphean Sumsunur granite batholith. The ore field is controlled by a deep fault, which extends for up to 7 km at a width of 400 m and is expressed in steep shear and cataclasis zones. The orebodies are mineralized zones and more rare stockworks and veins surrounded by relatively thin aureoles of listwanite, beresite, and silicified rocks. The major ore minerals are pyrite, chalcopyrite, sphalerite, pyrrhotite, gold, and electrum. Geochemical data on the rocks, metasomatites, and orebodies indicate that gold could have been borrowed from rocks of the Archean basement (amphibolites of the Gargan block) and rocks of the ophiolite complex, Proterozoic carbonaceous shales, and granitoids. According to the mineralogy and geochemistry of the deposit, it may be assigned to the cellular–floor type of zoning.

The Dal'nee and Oroch deposits in the Evenskoe ore field at the northern shore of the Sea of Okhotsk are hosted in the central part of the Cretaceous Okhotsk–Chukotka Volcanic Belt (OCVB) and are structurally restricted to central volcanic–tectonic edifices. The ore mineralization belongs to an epithermal low-sulfide vein type and was formed at a continental marginal mobile zone of the Pacific segment, the largest of which is OCVB. The Au–Ag ores of this deposit are noted for high Ag contents [7].

The Pokrovskoe Au–Ag epithermal deposit in Amur oblast is localized in the western flank of the Late Mesozoic Umlekan–Ogodzhin volcano-plutonic belt. The deposit is restricted to the Tygda–Sergeevskii intrusion-dome uplift in its junction zone with the Ulunginskaya depression in the marginal part of the Sergeevskii granitoid massif. The orebodies of the deposit often have no clear-cut boundaries. These are variably silicified (up to the development of filling veins) argillized volcanic rocks and granitoids. The ore mineralization at the Pokrovskoe deposit is characterized by the predominance of Au over Ag [8].

Concentrations of major ore admixtures in pyrite from our samples (data of semiquantitative atomic-emission analyses conducted at the Vinogradov Institute of Geochemistry are reported in Table 1.

The electron spectroscopic techniques used in studing pyrite crystals (x-ray photoelectron spectroscopy XPS and Auger electron spectroscopy AES, respectively) were considered in detail in [4], and much of our AES data was presented in [1]. Our research was conducted on euhedral crystals ranging from ~0.5 to 1 mm in size in order to carry out analysis at the natural surface of crystal faces but not randomly oriented fractures [4]. This strongly limited the number of samples suitable for our research. Control measurements at larger and smaller fractions of some of our samples proved that the results are consistent within the analytical error and that the position of the XPS peaks are invariant to within ±0.2 eV. The data of Table 2 pertain to samples with the most clearly pronounced peaks. The analysis of the crystal surfaces was conducted on a LAS-3000 (Riber) spectrometer equipped with an OPX-150 hemispherical retarding-field electron-energy analyzer and an Auger electron spectrometer with a cylindrical mirror analyzer. Atoms at the surface of the samples were excited by x-ray radiation from an Al anode (Al K_α = 1486.6 eV) at an emission current of 20 Ma and a tube voltage of 10 kV. The vacuum in the analytical chamber was 5×10^{-10} Torr. The spectra were calibrated on the C 1*s* line of C with a binding energy of 285 eV. The spectra were standardized using the line $4f_{7/2}$ of Au at 84.0 eV. The spectra were processed with a specialized computer program relative to the nonlinear background. The geometries of the peaks are approximated by a mixed Lorentz–Gaussian function. The atomic concentrations of the elements and their various species were calculated from the areas beneath the peaks accu-

Table 1. Concentration (ppm) of major admixtures of ore elements in our pyrite samples (data of semiquantitative atomic emission analysis)

Sample	Locality	Mn	Ti	Ni	Co	W	Pb	Cu	Zn	Cd	As	Sb	Bi	Ag	Au
Level 1540	Zun-Kholba	20	50	10	6	10	750	3000	1300	10	2500	150	90	50	140
Pioner-skaya	"	10	40	10	60	n.d.	30	600	350	n.d.	750	n.d.	12	30	160
NT7/4	"	30	20	50	40	30	4000	200	8000	10	600	2	10	15	8
NTR 12/18.5	"	40	50	30	60	10	80	30	20	n.d.	50	n.d.	10	5	n.d.
510/1	Pok-rovskoe	100	200	30	20	n.d.	300	50	100	n.d.	5000	300	200	100	2
K-24	Oroch	20	50	30	20	n.d.	3000	480	1400	n.d.	200	n.d.	n.d.	1670	130
R-1953	Dal'nee	n.d.	n.d.	70	110	n.d.	110	40	30	n.d.	280	n.d.	n.d.	20	2

Note: n.d. – not detected (concentration below the detection limit).

rate to ±10%. The surface of the samples was etched by a beam of Ar ions with an energy of 2 keV and an emission current of 20 mA. For this purpose, the analytical chamber was filled with Ar under a pressure of 2×10^{-5} Torr.

The topography of the crystal faces was examined on an SMM-2000 (Russia) scanning multimicroscope in scanning tunnelling microscopy (STM) and atomic force microscopy (AFM) contact modes. Most measurements were carried out in the STM mode, which provides more realistic imagery of a surface with resolution up to a few Ängstöms at solid samples. The software of the microscope makes it possible to analyze the roughness and other characteristics of a surface and determine the heights and shapes on nanometer-sized features on the surface.

RESULTS

Characteristics of pyrite crystal samples and the results obtained on their spectra are presented in Table 2. For the sake of brevity, this table does not report less important details, such as the characteristics of the less intense component $2p_{1/2}$ of the S $2p$ doublet and the relations between the Lorentz and Gauss functions during the deconvolution of the peaks. The attribution of the peak is described in detail in [4] and we will not repeat the reasoning here.

The most important issues related to the typochemistry of crystal surfaces are, first, the differences between pyrite from shallow-depth epithermal Ag–Au deposits and from the deeper mesothermal Au deposit (Zun-Kholba). The differences were both qualitative and quantitative in nature. The data of Table 2 demonstrate that sulfoxi anions at pyrite from the Zun-Kholba deposit are mostly sulfite, whereas these anions in pyrite from mesothermal deposits are dominated by the sulfate ion. Pyrite from the Zuk-Kholba deposit is characterized by high S/S_2 ratios at the surface, particularly in the sample from a deep level at the mineralized zone (Table 1, Level 1540). This ratio is ~3.7 and not only does not decrease but even slightly increases after ion etching, as is shown in Fig. 1. This figure also displays the disappearance of the peaks of the sulfate ion (a and c) and a notable redistribution of the intensities of the peaks corresponding to various Fe species (b and d) after etching for 1 h. Recall that the procedure of obtaining the S/S_2 ratio from unresolved spin-orbital $2p_{3/2-1/2}$ doublet is not flawless [4] and represents only a very rough approximation. It can be definitely concluded only that the surface layer of pyrite from the Zun-Kholba deposit is fairly thick (more than ~400 nm). A notable decrease in the intensity of the Fe peak of the NP and the corresponding increase in the intensity of the FeII peak of "volume" pyrite (Figs. 1b, 1d) after etching indicate that the NP was removed from the surface. Data of scanning probe microscopy enabled us to visualize this phase (Fig. 2a) and determine its principal parameters [4]: the maximum height of the "topographic" features, the mean area roughness (mean roughness over an area), and the fractal dimension of the surface. The corresponding values are 570 nm, 80 nm, and 2.075, respectively. For pyrite from an exposed mineralized vein (Table 2, Pionerskaya), the situation is somewhat different (Fig. 3). The surface contains trivalent Fe, and its phase (perhaps, FeOOH) partly overlaps PoNP. The absence of oxidized S species on the surface (Figs. 3a, 3c) suggests that pyrite has in this case an oxide or oxi-hydroxide cover [9]. Etching leads to a significant decrease in the concentration of FeIII because of the removal of the oxide phase of FeIII (Figs. 3b, 3d) and the exposure of the NP, as follows from the greater clearness of the Fe peak of PoNP (~710 eV). This scenario finds certain support in Fig. 2b, which shows two types of surface features of different size in the pyrite crystal from this sample. The morphological characteristics suggest the presence of only fragments of ordering in the PoNP nanostructure

Table 2. XPS data on natural pyrites

№/назв. пробы	Locality	Setting, size *, and crystal morphologies	XPS data **							
			Fe $2p_{3/2}$				S $2p_{3/2}$			
			E, eV	W, eV	Peak attribution	at %	*E,* eV	W, eV	Peak attribution	at %
Level 1540	Zun-Kholba	Orebody, depth level 0.5–1.0, {100}	706.0 710.3	3.6 5.0	FeII–S_2 FeII–S(np)	39 61	161.5 163.0 165.5	3.0 2.3 2.7	S S_2 SO_3	67 18 15
			etching for 1 h							
			706.4 709.6	3.7 5.0	FeII–S_2 FeII–S(np)	58 42	160.4 162.2	2.2 2.4	S S_2	82 18
Pionerskaya	″	Orebody, surface 0.5–1.5, {100}	706.5 710.0 712.6	3.3 6.5 5.0	FeII–S_2 FeII–S(np) FeIII–SO_3, FeIII–O,OH	35 40 25	161.5 162.9 165.5	2.6 2.6 2.0	S S_2 SO_3	63 26 11
			etching for 1 h							
			706.3 709.1 713.0	3.6 4.8 5.0	FeII–S_2 FeII–S(np) FeIII–O,OH	42 39 19	160.5 162.0	2.8 2.3	S S_2	76 24
NT7/4	″	Orebody, intermed. level 0.3–2.0, {100}	706.3 710.4	6.0 5.0	FeII–S_2 FeII–S(np)	38 62	160.8 162.8 166.3 168.5	2.6 2.3 2.3 2.3	S S_2 SO_3 SO_4	35 27 23 15
NTR 12/18.5	″	Wall-rock metasomatite, intermed. level 0.4–3.5, {100}	706.1 710.0	3.7 2.9	FeII–S_2 FeII–S(np)	77 23	161.3 163.0 166.5	2.6 2.7 4.0	S S_2 SO_3	46 39 15
510/1	Pokrovskoe	Wall-rock metasomatite, 0.2–2.0, {100}	Poor spectrum resolution (admixtures ?)				161.2 162.6 168.5	2.0 2.0 3.5	S S_2 SO_4	50 16 34
K-24	Oroch	Orebody, depth level 0.4–1.5, {100} {hk0}	707.7 710.3 712.5	2.0 4.5 4.0	FeII–S_2 FeII–S(нф) FeIII–SO_4	8 71 21	161.0 162.5 164.0 168.0	2.5 2.5 1.5 3.1	S S_2 S^0 SO_4	8 32 5 55
R-1953	Dal'nee	Orebody, 0.3–0.6, {210}	710.2 712.0 713.1	4.2 6.0 5.2	FeII–S(np) FeIII–SO_3 + + FeIII–S_2O_3? FeIII–SO_4	45 35 20	160.0 161.5 166.3 169.3	2.0 3.0 3.0 3.0	S S(S_2O_3)*** SO_3, S_2O_3 SO_4	25 20 28 27
			etching for 1 h							
			no data				161.2 162.5 168.0	2.6 3.5 5.0	S S_2 SO_4	34 25 41

Notes: * polyhedron edge, mm;

** *E* is the binding energy, eV, W, total peak width at half of its maximum height; see text and [4] for peak attributions; at % were calculated assuming that all species of a given element amount to 100%;

*** S^{2-} sulfur in the thiosulfate ion.

observed at the previous sample (Fig. 2a). This is numerically pronounced as differences in the surface characteristics at its discrete sites. Where overlapped with an oxide film, the maximum height of the features is ~50 nm, the mean area roughness is ~9 nm, and the fractal dimension is 2.015. Within smaller areas of the granular nanostructure (we attribute them to PoNP), these characteristics (on average) are ~140 and ~26 nm

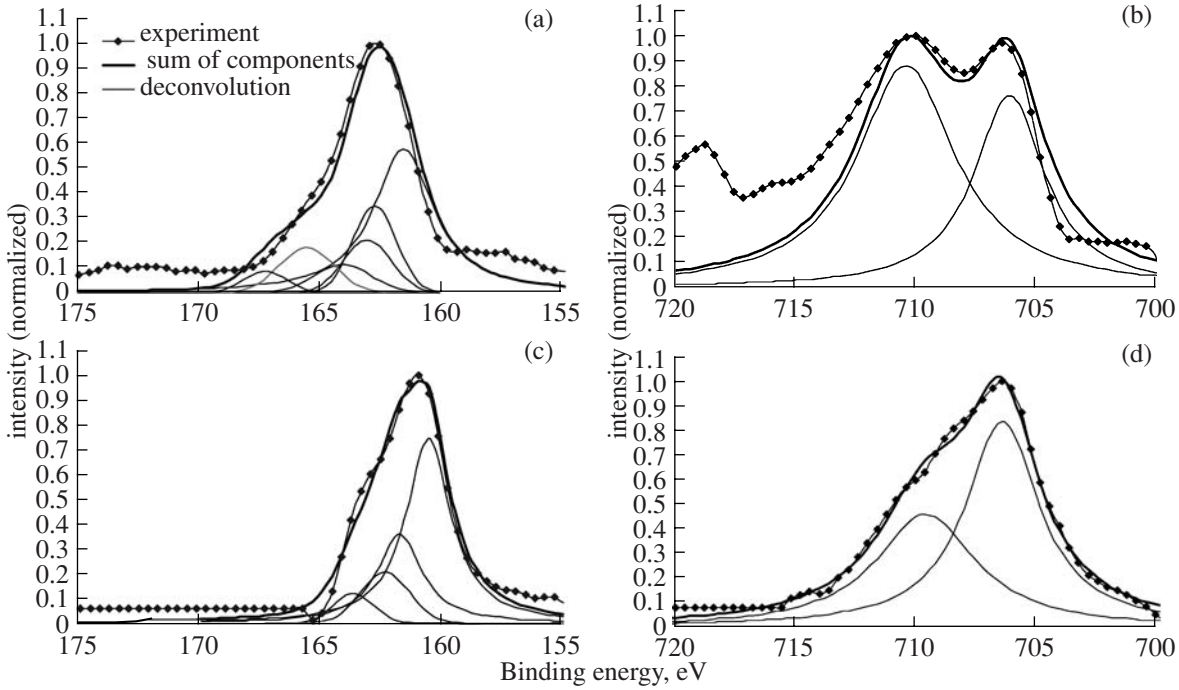

Fig. 1. XPS spectra of (a, c) S *2p* and (b, d) Fe $2p_{3/2}$ for pyrite crystals from a mineralized vein at a deep level of the Zun-Kholba deposit (Table 1, sample Level 1540).

(a, b) Original sample; (b, c) Ar^+ etching for 1 h.

Sulfide sulfur dominates over sulfate sulfur. Ion etching partly purified the surface of FeII NP and completely of the sulfate ion.

and 2.057, respectively, and approach the values typical of PoNP of synthetic hydrothermal pyrite [4]. Note that all of the figures are rounded off for a number of scans and, within each scan, for a number of sites. Pyrite crystals from metasomatic wall rocks at the Zun-Kholba deposit are noted for the less significant development of the NP at the surface than that on pyrite from the orebodies. This is expressed in a decrease in the relative intensity of the FeII-S peak of the NP (Figs. 4b, 4d). The S anion speciation also becomes simpler (compare Figs. 4a and 4c). In this instance SPM does not detect any significant ordered nanometer-sized features on the surface except single features (Fig. 2c) with a maximum height of ~100 nm. The mean area roughness of individual scans varies from ~15 to 30 nm (~2–5 nm at flat areas), and the fractal dimension ranges from 2.006 to 2.009. Obviously, these characteristics differ strongly from those reported above for pyrite from the mineralized vein, as can also be clearly seen when the scans in Figs. 2a and 2c are compared.

Pyrite samples from epithermal Au–Ag deposits are spectroscopically different from pyrite from the Zun-Kholba mesothermal deposit in two respects: (1) they have high-intensity peaks of the most oxidized S species (sulfate ions, Figs. 5a, 5c, 5d) and weak (Fig. 5b) (if any) peak of FeII–S_2 of "volume" pyrite at 707 nm. At the same time, the *2p* spectrum of S in Fig. 5c closely resembles the S spectrum in Fig. 4a, which likely suggests similar conditions under which ore mineralization developed at these genetically different deposits and, consequently, NPs of more complicated composition (Fe[S, S_2, SO_3, SO_4]), which is characterized by a stronger ability to accommodate admixture elements [1]. Precisely what these conditions were may be established by a comparison with experimental results [4]. Sulfate appears in high enough concentrations in the surface during crystallization in a system with Zn sulfide at a relatively low S fugacity. In this case, the latter parameter can be evaluated from the FeS concentration in sphalerite coexisting with pyrite in sample NT7/4: 9.6 mol %. Assuming the crystallization temperature of this association to be approximately 400°C and using the well known equation from [10], we arrive at $\log f_{S_2} = -7.6$ bar. The analogy with experimental data is also apparent when the spectra include an FeIII peak (binding energy ~713 eV). As was mentioned above, the data of Auger spectroscopy [1] indicate that pyrite from orebodies at epithermal Au–Ag deposits is characterized by elevated contents of admixture elements in the surface layers. For example, a K admixture, which is unusual in ore minerals, was detected in sample K-24, whose surface contains as much as 8 at % K. The presence of K was traced to a depth of ~400 nm, i.e., practically throughout the whole thickness of the NP layer. Another admixture is Ag (up to ~5 at %), which is also concentrated within a ~0.5-μm-thick surface layer. Sample R-1953 (Table 2) is characterized by the presence of Tl and Cu admix-

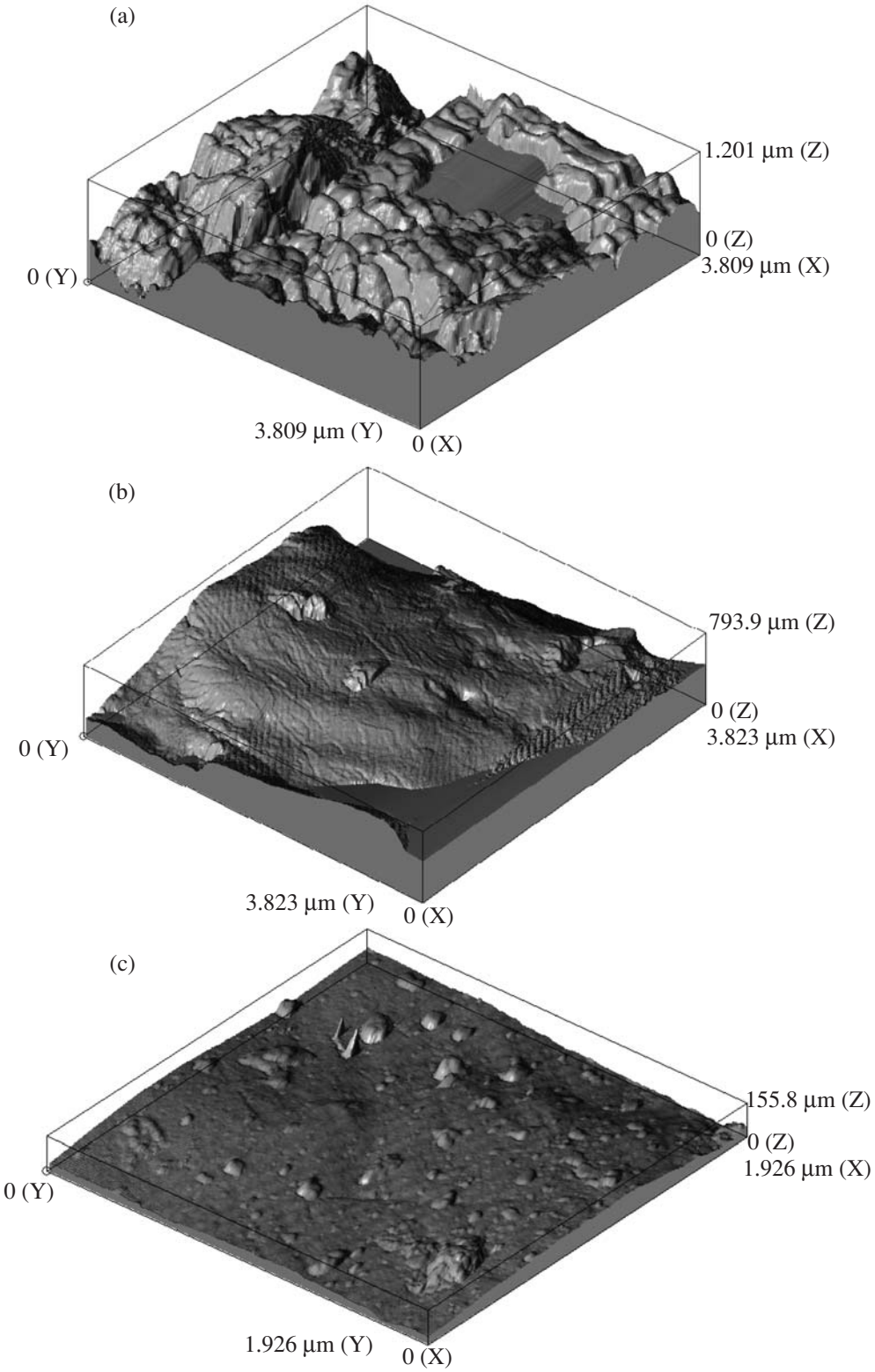

Fig. 2. 3D atomic-force microscopic imagery of the surface of pyrite crystals from the Zun-Kholba deposit (Table 1).
(a) Level 1540, scan $3.809 \times 3.809 \times 1.201$ μm; (b) Pionerskaya, scan $3.823 \times 3.823 \times 0.794$ μm; (c) NTR12/18.5, scan $1.926 \times 1.926 \times 0.156$ μm

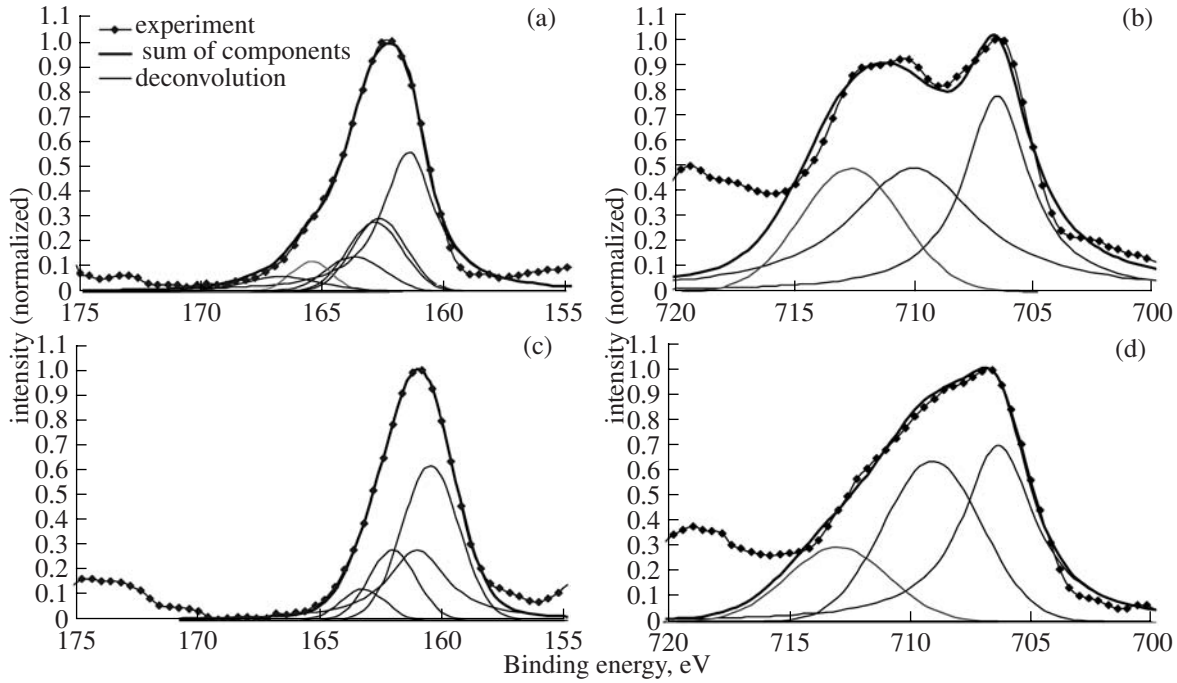

Fig. 3. XPS spectra of (a, c) S 2*p* and (b, d) Fe $2p_{3/2}$ for pyrite crystals from an orebody exposed at the surface at the Zun-Kholba deposit (Table 1, Pionerskaya sample).

(a, b) Original sample; (c, d) Ar^+ etching for 1 h.

Oxidized S species are practically absent from the surface. The peak of FeII NP is pronounced more clearly after etching, the intensity of the FeIII peak decreases. FeIII occurs in an oxide or oxi-hydroxide mode.

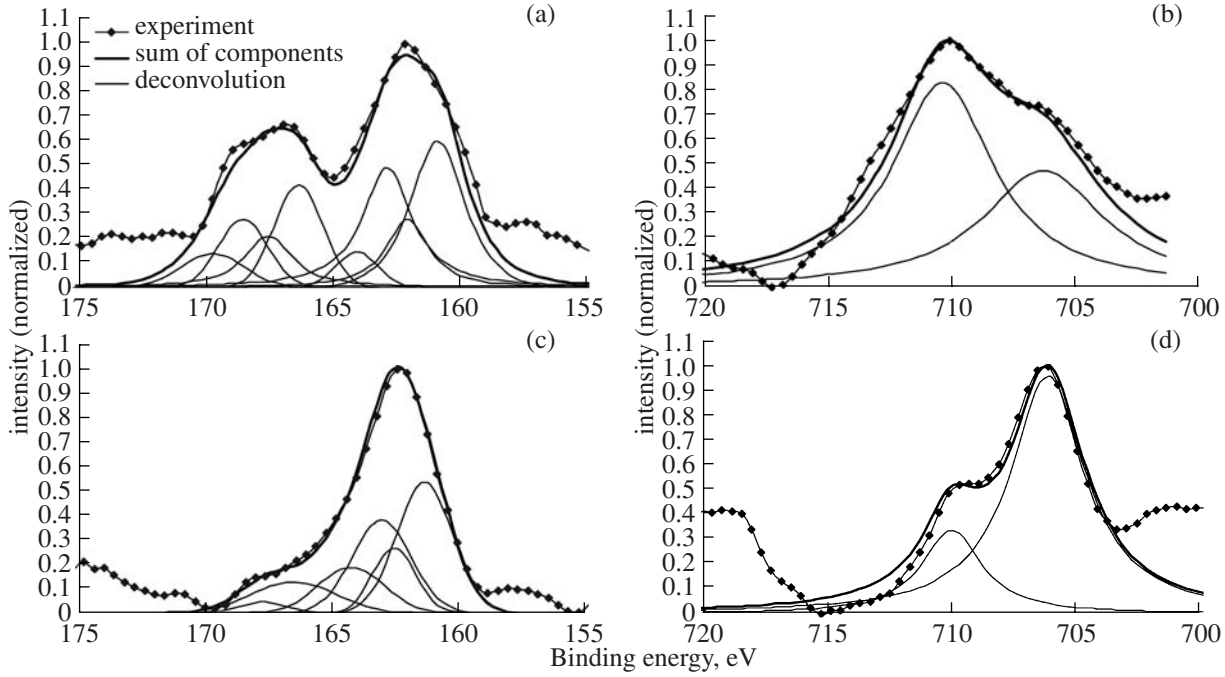

Fig. 4. XPS spectra of (a, c) S 2*p* and (b, d) Fe $2p_{3/2}$ for pyrite crystals from the Zun-Kholba deposit: (a, b) an orebody (Table 1, sample NT7/4) and (c, d) wall-rock metasomatite (Table 1, sample NTR12/18.5).

The FeII peak in NP has a low intensity for pyrite from the metasomatic rock, which suggests that the NP is poorly developed. The surface of pyrite from the orebody is characterized by a broad spectrum of S species: S^{2-}, S_2^{2-}, SO_3^{2-}, and SO_4^{2-}.

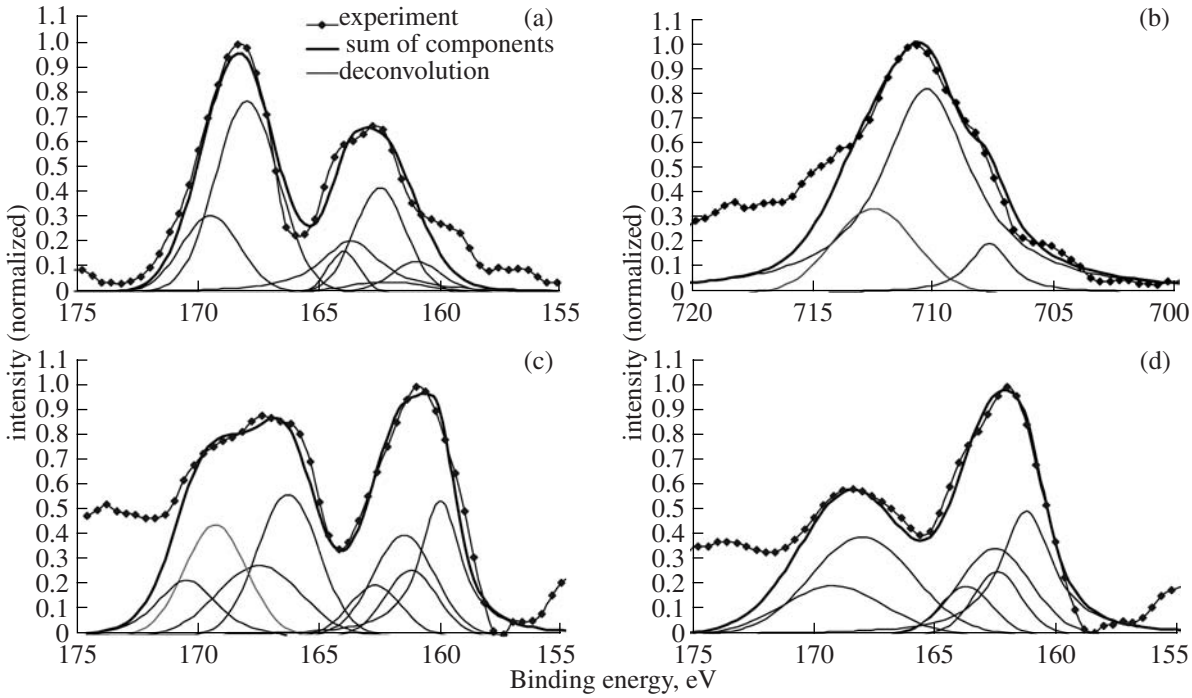

Fig. 5. XPS spectra of (a, c, d) S 2*p* and (b) Fe $2p_{3/2}$ for pyrite crystals from epithermal Au–Ag deposits in northeastern Russia: (a, b) Oroch (Table 1, sample K-1) and (c, d) Dal'nee (Table 1, sample R-1953, 1 h etching).

Note analogous distributions of sulfur species in the orebodies at (c) Dal'nee and Zun-Kholba deposits (Fig. 4, a), although some S^{2-} is in this instance a component of the thiosulfate ion. Note the high sulfate concentration in the surface layer (a) and the subsurface layer (d) and the predominance of the peak of FeII in NP, which testifies to the maximum development of the NP on the surface.

tures [1]. Their concentrations in a surface layer ~400 nm thick are so high that these elements are readily identified based on peaks in XPS spectra (Fig. 6). Tl is most probably contained in the surface layer in the form of sulfide (Fig. 6a), as is most of the Cu (~56 at %, Fig. 6b). Approximately 16 at % Cu may be contained in chalcopyrite with ~28 at % in the form of a sulfide. Such anomalies of the accommodation of minor elements can be explained by structural features and the structure of chemical bonds in the nonautonomous surface phase. SPM data on sample K-24 indicate the presence of a two-level nanostructure, which resembles the nanostructure of an NP on pyrrhotite synthesized by hydrothermal crystallization in the presence of Cd sulfide [11]. Because of its interesting nanostructure, this sample was examined particularly thoroughly. We identified and studied areas with the predominance of a "small" structure (Fig. 7a), areas with the predominant development of larger ordered features (Fig. 7b), and areas of perfectly flat surface surrounded by aggregates of features of various sizes (Fig. 7c). The parameters of these features significantly vary and suggest that they could be formed by more than one NP. On the flat surface (Fig. 7c), which is interpreted as the natural surface of an ideal crystal face of an equilibrium form, the roughness does not exceed 1 nm, the maximum height of the features is ~20 nm, and the fractal dimension is ~2.002. The "small" structure is characterized by the following corresponding parameters: ~8–14 nm, ~60–100 nm, and ~2.006–2.015, whereas the "large" structure has ~10–30 nm, ~100–150 nm, and ~2.030–2.050. The small overlap of the parameter (or even the absence of an overlap for the fractal dimension) suggests that the surface bears at least two types of NPs.

DISCUSSION

The nonstoichiometric character of the surface of natural pyrite samples was described in our earlier paper [1], which was devoted to pyrite samples from the same deposits that were examined chiefly by Auger spectroscopy with ion etching of the surface. The (S + O)/Fe ratio varied from ~1.2 to ~2.3, most of the points falling within the range of 1.4–2.0, thus marking a shift in the composition toward FeS. Because of the more significant oxidation of natural pyrites compared to that of synthetic pyrites [4] and the absence of data on the state of Fe, it was concluded [1] that the NP on the hydrothermal pyrite is of pyrrhotite character, although the principal conclusion of the occurrence of an NP had already been reached. It was mentioned that pyrite from the Zun-Kholba deposit is less oxidized compared to that from epithermal deposits, although this research touches not only upon the quantitative aspect of the problem (lower oxygen concentrations in the surface) but also on its qualitative aspect (the predominance of

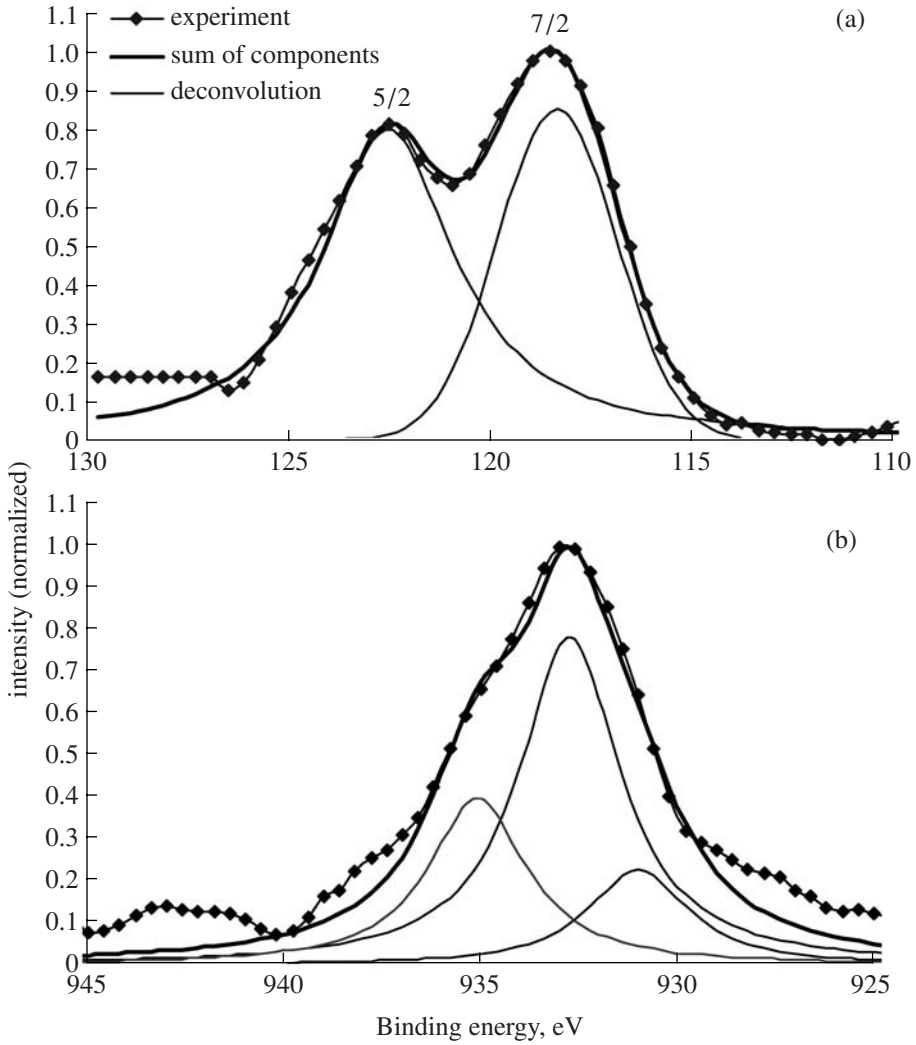

Fig. 6. XPS spectra of (a) Tl 4*f* and (b) Cu 2*p* for pyrite crystals from the Dal'nee epithermal Au–Ag deposit (Table 1, sample R-1953).

The T1 doublet at 118.3–122.5 eV corresponds to a sulfide mode of this element. The occurrence of three Cu $2p_{3/2}$ peaks (at 931.0, 932.7, and 935.1 eV) testifies to the presence of three modes of Cu occurrence: chalcopyrite, sulfide, and sulfate in an approximate proportion of 1 : 4 : 2.

tetravalent S over sexavalent S). The occurrence of FeIII–O, OH bonds and a FeIII oxi-hydroxide or oxide film on pyrite crystals characterize the conditions of supergenesis. Oxi-hydroxide covering films were identified by XPS on the surface of pyrite affected by mine waters [9]. The paragenetic succession includes earlier patchy and later massive (not structured) films with a population of crystalline FeIII oxi-hydroxides in between. It is interesting to note the absence of FeIII sulfate on the pyrite surface even in remarkably oxidized environments at the Earth's surface or where affected by mine waters. We believe that one of the possible reasons is the stability of the underlying oxi-hydroxide layer of an NP and the instability of simultaneously existing sulfate and disulfide ions [4], which result in the wide development of sulfite (Table 2, Zun-Kholba deposit and data on synthetic hydrothermal pyrite in [4]). In contrast, pyrites from epithermal Au–Ag deposits exhibit sulfate on their surface, which is an indicative typochemical feature of low-temperature epithermal ore mineralization. The reason for this difference is still largely obscure. Conceivably, it is related to the mechanism of pyrite oxidation. It was demonstrated in [12] that the "purely surface" S-bearing components of pyrite that are in contact with atmospheric gases undergo oxidation to sulfate, whereas "volumetric" S produces mostly electron-deficient disulfides or polysulfides. If pyrite oxidation takes place in an aqueous solution at a low pH value, the continuous removal of reaction products by their dissolution results in continuous "refreshing" of the surface and the exposure of new S atoms accessible to dissolution at the surface. If overlying FeOOH layers develop (at alkaline pH), electron-deficient di- or polysulfides are formed

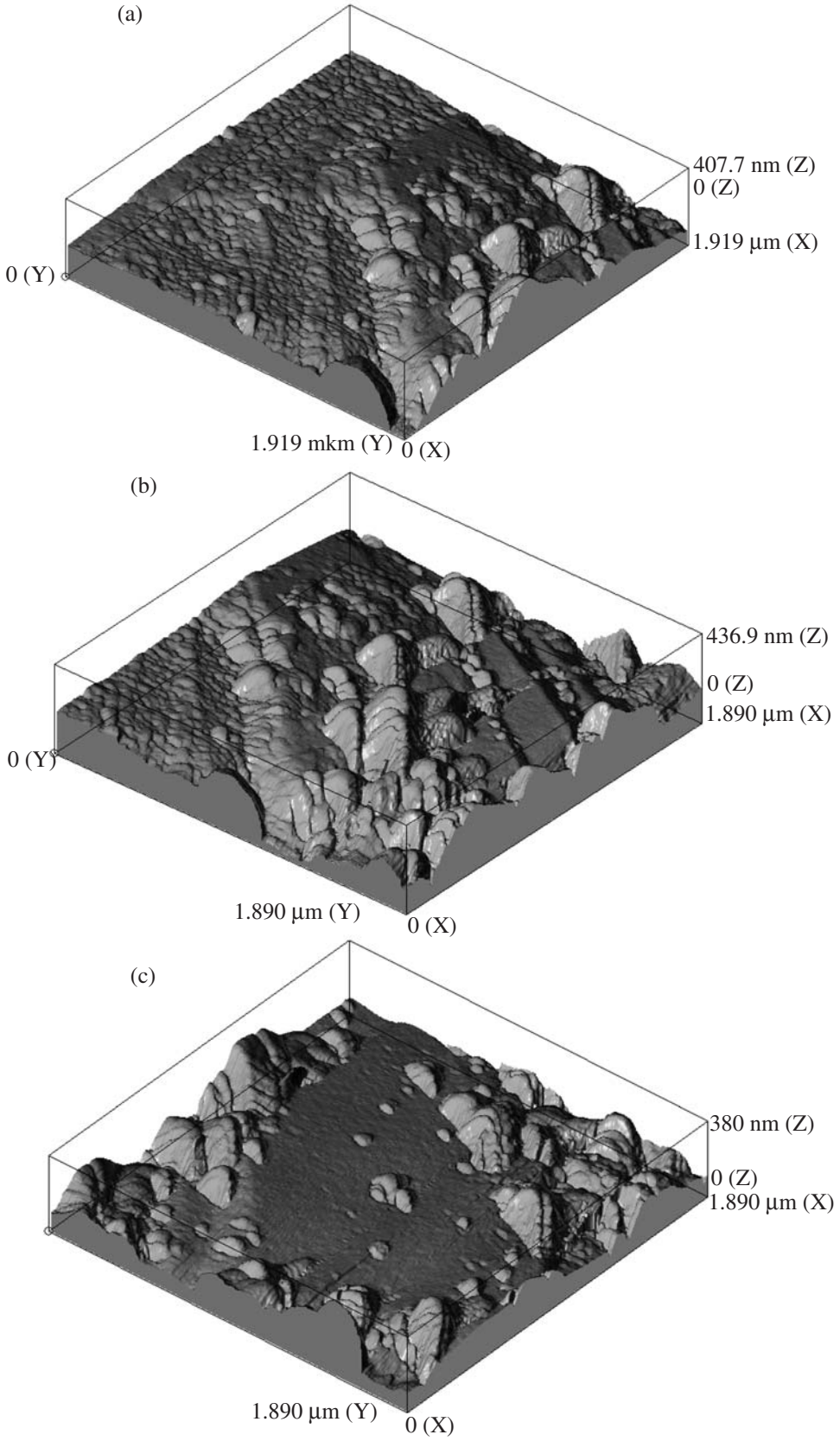

Fig. 7. 3D atomic-force microscopic imagery of the surface of pyrite crystals, sample K-24 from the Oroch deposit (Table 1). Scans: (a) 1.919 × 1.919 × 0.408 μm; (b) 1.890 × 1.890 × 0.436 μm; (c) 1.890 × 1.890 × 0.380 μm

[12]. While reasonable, this explanation is nevertheless at variance with experimental data [4]. The growth of pyrite crystals occurs with continuous "refreshing" of their surface in solutions with relatively low pH but does not bring about any significant sulfur oxidation to sulfate. Moreover, it is hard to understand why this transformation is not completed in nature. An alternative explanation relies on the occurrence of a thick layer of an NP on the surface of low-temperature pyrite from epithermal deposits, with this pyrite crystallizing in the presence of admixture components (Zn, Pb, As, K, Cu, Tl, Ag, and others). The presence of additional elements, many of which are univalent, facilitates valence compensation of FeIII in the NP via the development of clusters (pseudo-end members of the "solid solution") like $AgFeS_2$, $KFeS_2$, $TlFeS_2$, and $CuFeS_2$, which are known as individual mineral species or chemical compounds [13–15]. Trivalent elements (chiefly,l As) can also be concentrated in the surface layer of the NP by substituting Fe^{3+} for these elements or by forming clusters (FeAsS) binding excess Fe^{3+} in the NP. Transition metals are similarly adsorbed on goethite with the development of surface precipitates with the substitution of Fe^{3+} in the structure [16]. It was determined that the compositions and properties of NPs may notably differ for pyrites from mesothermal and epithermal deposits: the former are close to those of PoNP found on synthetic hydrothermal pyrites [4] and containing an additional sulfate anion, and the latter are close to those of sulfide–disulfide–sulfate compositions with trivalent Fe. In fact, this NP is a sulfoxide phase able to accommodate high concentrations of admixture elements, including precious metals, because of the stabilization of clusters with Fe^{3+} and, perhaps, also SO_4^{2-} in the nonrigid structure of the NP. The latter are widely known in, for example, the "loose" structures of aluminosilicate phases in lazurite and other sodalite-like minerals (clusters of $[Na_3CaSO_4]^{3+}$ and others [17]. The conditions under which this phase can be formed are still poorly known, though apparently it likely formed in multiphase systems with other sulfides (ZnS) at relatively low S fugacity (near the pyrite–pyrrhotite buffer). In experiments on the chemical etching of natural pyrite, sulfide appears in appreciable concentrations under the effect of strong oxidizers, such as K permanganate, due to the disproportionation of the disulfide ion and the generation of free S [18]. Conceivably, these conditions were close to those of sample K-24 (Table 1), although the concentration of detected S^0 is very low and can be incorrectly determined.

The size parameters of the surface features obtained with SPM for natural pyrites are consistent with data on synthetic hydrothermal pyrites and the results obtained by other techniques (XPS, Auger spectroscopy, and ion etching), although the NP layer can be slightly thicker than that on synthetic pyrite or thinner and fragmentary (an example is pyrite from the Zun-Kholba deposit); this layer can also be overlain by oxidation products of oxide or oxi-hydroxide composition. Nevertheless, in speaking of a chemically modified layer and an NP contained in it, we definitely mean a nanostructure in the surface layer of a crystal about 0.5 μm thick. This confirms our earlier conclusion [4] that the surface heterogeneity in which the typochemistry of mineral surfaces can be expressed is submicrometer (nanometer) sized. Further support is also provided for the suggestion [4] that the NP on pyrite surface can play an important geochemical role during the accommodation of trace elements incompatible with the pyrite structure but relatively easily adjustable to the less rigid structure of the NP. If an analogy is drawn with the NP in the system pyrite–CdS [11] and the curved geometry of crystal faces in sample K-24 is recalled, it can be hypothesized that the "small" structure (Fig. 7a) develops at vicinals because of their morphological instability with respect to the development of nanometer-sized topographic features of the hill and valley type [19]. The surface acquires thereby a facetted nanostructured shape in the form of ordered domains coherently juxtaposed with the surface of the crystal face. As it is in the state of elastic deformation, such domains may improve their stability via the excess dissolution of both cation (K^+, Ag^+, and Au^+; Table 1) and anion (SO_3^{2-}, and SO_4^{2-}, Table 2) admixtures or a transition into another phase state (PoNP). In addition, and probably as a result, nonautonomous "precursor" phases like $AgFeS_2$, $KFeS_2$, and $CuFS_2$ form on the crystal surface, with these phases crystallizing outside their stability fields, "in volume", like cubic CdS on pyrrhotite [11]. These can also be two different types of NPs that provide a basis for the double-level nanostructure on the surface of pyrite crystals from the Oroch epithermal Au–Ag deposit (Fig. 7).

The fact that elevated Au concentrations are restricted to the surface of pyrite crystals [20] can be clearly traced at numerous deposits and can be caused by the accommodation of this element by an NP whose partition coefficient (K_p) of Au is higher than that of "volume" pyrite [21]. Data [22] on an increase of the integral K_p of Au between pyrite and hydrothermal solution in a system with As and the ensuing generation of the NP [4] provide further support for this suggestion. An experimental test involves a fairly complicated procedure for the determination of the real (for structural Au) and apparent (i.e., caused by accommodation at the surface) partition coefficient. This problem will be the subject of our future research.

As regards natural pyrites, it should be noted that, unfortunately, the data presented in this paper cannot be considered statistically representative and highlights only the principal tendencies in the typochemistry of pyrite surface. For example, an interesting phenomenon is the weak development of NP on pyrite from wall-rock metasomatites, a fact confirmed by SPM data (Fig. 2c). Comparison with experimental results [4] indicates that this situation can take place in two

instances. First, if the pyrite crystallizes in a sufficiently pure system, in the absence of additional phases (including virtual phases) crystallizing concurrently with it, i.e., in the absence of the potentially possible phases of admixture elements (because they can indirectly affect the synthesis of NP, which are regarded as "precursor" phases [23]). Second, if crystallization takes place at an elevated S fugacity. A decisive solution of such issues, which will shed light on the chemical differences between the mechanisms forming ore mineralization in orebodies and metasomatic rocks [20], is possible only with the accumulation of a sufficient volume of empirical data.

CONCLUSIONS

1. Data obtained on pyrite crystals from deposits of various genesis (mesothermal quartz–sulfide gold and epithermal low-sulfide gold–silver) confirm our earlier conclusion, drawn from results of hydrothermal experiments [4], that there exists an NP of variable composition on the crystal surface that provides a record of the conditions under which the crystals grew.

2. The lower oxygen concentration on the pyrite surface from the Zun-Kholba gold deposit and the higher degree of sulfur reduction at this surface (the predominance of tetravalent sulfur over sexavalent sulfur) compared to pyrites from gold–silver deposits implies that deep mesothermal ore mineralization that had no links to the surface was produced under more reduced conditions. The development of sulfate on the surface of pyrites from epithermal gold–silver deposits is a typochemical feature of low-temperature, low-depth ore-forming processes.

3. Supergene conditions are characterized by the occurrence of FeIII oxi-hydroxide or oxide films on the surface of crystals, with these films being morphologically markedly different from the layer of a pyrrhotite-like NP.

4. Crystals of natural pyrite and those synthesized in hydrothermal experiments are characterized by submicrometer- (nanometer-) sized surface heterogeneities ($\leq$~0.5 μm) within which surface typochemistry is pronounced.

5. The composition and properties of the NPs differ for pyrites from deposits of different genesis. These phases on the mineral from a mesothermal quartz–sulfide deposit are close to a pyrrhotite-like NP that was discovered on synthetic pyrites and contained additional sulfite anions. The latter phase from epithermal gold–silver deposits is close to sulfide–disulfide–sulfate ensembles with trivalent iron. The incorporation of admixtures (including precious metals) in this phase can take place via the stabilization of clusters with Fe^{3+} and SO_4^{2-}. in its structure.

6. The instability of the crystallization process in epithermal environments may trigger the development of a double-level nanostructure because of the restructuring of vicinal surfaces into an ordered system of domains and the synthesis of "precursor" phases. Such systems can be stabilized by means of the excess dissolution of admixtures or the transition of the surface layer into another phase state (because of a process similar to polymorphic transition).

7. The spectrum of examined mineral crystals should be broadened to obtain statistically representative data on the surface of natural pyrite crystals. Further experimental research is needed to determine the capture coefficients of admixtures by nonautonomous surface phases.

ACKNOWLEDGMENTS

The authors thank Yu.V. Shchegol'kova for help in the spectroscopic research. This study was financially supported by the Russian Foundation for Basic Research (project no. 06-05-64171) and a grant from the Siberian Branch, Russian Academy of Sciences (Integration Project 96). The equipment of our SPM was provided by Rossnauka in 2004 under the Program for the Support and Maintenance of Equipment for Research Organizations.

REFERENCES

1. V. L. Tauson, R. G. Kravtsova, and V. I. Grebenshchikova, "Chemical Typomorphism of the Surface of Pyrite Crystals of Gold Ore Deposits," Dokl. Akad. Nauk **399**, 673–677 (2004) [Dokl. Earth Sci. **399**, 1291–1295 (2004)].
2. V. L. Tauson and R. G. Kravtsova, "Chemical Typomorphism of the Mineral Surface: Compositional Specifics of the Surface: An Example of Gold-Bearing Pyrite from Epithermal Deposits," Geol. Geofiz. **45** (2), 222–227 (2004).
3. G. B. Naumov, "Current Relations between Mineralogy, Geochemistry, and Physical Chemistry," in *Theory and Methodology of Mineralogy* (Komi FAN SSSR, Syktyvkar, 1985), Vol. 1, pp. 23–24 [in Russian].
4. V. L. Tauson, D. N. Babkin, E. E. Lustenberg, et al., "Surface Typochemistry of Hydrothermal Pyrite: Electron Spectroscopic and Scanning Probe Microscopic Data. I. Synthetic Pyrite," Geokhimiya, No. 6, 615–628 (2008) [Geochem. Int. **46**, 565–577 (2008)].
5. V. L. Tauson and N. V. Smagunov, "Composition of the Surface of Pyrrhotite ($Fe_{1-x}S$) Crystals Synthesized in Association with Greenockite (α-Cd,Fe)S) under Hydrothermal Conditions: Introduction into the Geochemistry of Nonautonomous Phases," Geokhimiya, No. 4, 448–454 (2004) [Geochem. Int. **42**, 377–382 (2004)].
6. V. I. Grebenshchikova and A. P. Shmotov, "Stages of the Formation of the Zun-Kholba Gold Deposit, Eastern Sayan," Geol. Geofiz. **38** (4), 756–764 (1997).
7. R. G. Kravtsova, "Mineralogical–Geochemical Zoning and Formation of Gold–Silver Deposits (Russian Northeast)," Geol. Geofiz. **39** (6), 763–777 (1998).

8. V. G. Khomich, "Pokrovskoe Gold Deposit," in *Ore Deposits at Continental Margins* (Dal'nauka, Vladivostok, 2001), Part 3, No. 2, pp. 284–321 [in Russian].
9. H. W. Nesbitt and I. J. Muir, "Oxidation States and Speciation of Secondary Products on Pyrite and Arsenopyrite Reacted with Mine Waste Waters and Air," Mineral. Petrol. **62**, 123–144 (1998).
10. P. B. Barton, Jr. and B. J. Skinner, "Sulfide Mineral Stabilities," in *Geochemistry of Hydrothermal Ore Deposits*, (Wiley, New York, 1979), pp. 278–403.
11. V. V. Akimov, I. N. Gerasimov, V. L. Tauson, et al., "Microstructure and Chemical Composition of Nonautonomous Phases on the Surface of Crystals of Hydrothermally Synthesized Pyrrhotite ($Fe_{1-x}S$)," Surface and X-Ray, Synchrotron, and Neutron Studies, No. 12, 27–32 (2006).
12. A. G. Schaufuss, H. W. Nesbitt, I. Kartio, et al., "Incipient Oxidation of Fractured Pyrite Surfaces in Air," J. Electron. Spectrosc. Relat. Phenom. **96**, 69–82 (1998).
13. G. K. Czamanske, "The Stability of Argentopyrite and Sternbergite," Econ. Geol. **64**, 459–461 (1969).
14. H. Binder, "Die Anwendung der Rontgenphotoelectronenspectroskopie zur Klarung von Bindungsfragen in Eisen–Schwefelverbindungen," Z. Naturforsch., A: Phys. Sci. **28**, 255–262 (1973).
15. K. A. Sablina, V. V. Ikonnikov, and A. G. Klimenko, "Amorphization of $KFeS_2$ and $RbFeS_2$," in *Magnetic and Resonance Properties of Magnetic Dielectric* (Krasnoyarsk, 1985), pp. 194–206 [in Russian].
16. B. Singh, D. M. Sherman, R. J. Gilkes, et al., "Incorporation of Cr, Mn and Ni into Goethite (α-FeOOH): Mechanism from Extended X-Ray Absorption Fine Structure Spectroscopy," Clay Miner. **37**, 639–649 (2002).
17. I. Hassan and P. R. Buseck, "Incommensurate-Modulated Structure of Nosean, a Sodalite-Group Mineral," Am. Mineral. **74**, 394–410 (1989).
18. M. E. Fleet and S. L. Chryssoulis, and P. J. MacLean, "Arsenian Pyrite from Gold Deposits: Au and As Distribution Investigated by SIMS and EMP, and Color Staining and Surface Oxidation by XPS and LIMS," Can. Mineral. **31**, 1–17 (1993).
19. V. A. Shchukin and D. Bimberg, "Spontaneous Ordering of Nanostructures on Crystal Surfaces," Rev. Mod. Phys. **71**, 1125–1171 (1999).
20. V. Tauson, R. Kravtsova, and V. Grebenshchikova, "Surface Nature of Main Part of Invisible Gold and Estimation of Structurally Bound Gold in Pyrite of Gold Ore Deposits," in *12th Quadrennial IAGOD Symposium, Moscow, Russia, 2006. Program and Short Abstracts*, Ed. by S. V. Cherkasov (Moscow, 2006), No. 168.
21. V. L. Tauson, "Distribution of Ore Microcomponents between Mineral Crystals and Hydrothermal Solutions as a Method for Estimating the Metal Potential of Ore-Forming Fluids," in *Proceedings of International Conference on Topical Problems in Ore Genesis and Metallogeny, Novosibirsk, Russia, 2006* (Geo, Novosibirsk, 2006), pp. 218–219 [in Russian].
22. V. L. Tauson and N. V. Smagunov, "Influence of Associated Elements on Gold Behavior in the System Fe–S–Aqueous Salt Solution at a Temperature of 400°C and a Pressure of 100 MPa," Geol. Geofiz. **38** (3), 667–674 (1997).
23. V. L. Tauson, "Systematics of Processes of Trace Element Uptake by Real Mineral Crystals," Geokhimiya, No. 2, 213–219 (2005) [Geochem. Int. **43**, 184–190 (2005)].